Mechanics of Materials 172 (2022) 104390

Contents lists available at ScienceDirect

Mechanics of Materials

journal homepage: www.elsevier.com/locate/mecmat

Research paper

Fractional and fractal order effects in soft elastomers: Strain rate and temperature dependent nonlinear mechanics

Eugenia Stanisauskis [b,c], Somayeh Mashayekhi [a], Basanta Pahari [c], Markus Mehnert [d], Paul Steinmann [d,e], William Oates [c,*]

[a] Department of Mathematics, Kennesaw State University, Marietta, GA 30060, United States of America
[b] Department of Materials Science and Engineering, Florida State University, Tallahassee, FL 32310, United States of America
[c] Department of Mechanical Engineering, Florida A&M-Florida State University, Tallahassee, FL 32310, United States of America
[d] Institute of Applied Mechanics, University of Erlangen–Nuremberg, 5 Egerland Strasse, Erlangen, Germany
[e] Glasgow Computational Engineering Centre (GCEC), University of Glasgow, Glasgow G12 8QQ, United Kingdom

ARTICLE INFO

Keywords:
Fractional derivative
Viscoelasticity
Excluded volume
Zimm model
Fractal media

ABSTRACT

Soft dielectric elastomers are commonly used in applications where large deformation is prevalent such as energy harvesters, sensors, and soft actuators. The thermo-mechanical response of these elastomers is important in order to accurately describe the viscoelastic behavior over a broad range of operating conditions. Fractal characteristics of the dielectric elastomer VHB 4905 and their connection to fractional order viscoelasticity are analyzed to better understand viscoelasticity over a range of elevated temperatures starting at room temperature. We extend prior work in viscoelasticity to include excluded volume effects as a function of temperature. A fractal hyperelastic model is combined with a fractional order viscoelastic model and validated experimentally. Bayesian uncertainty methods are used to quantify the material parameters and their influence on temperature dependent viscoelasticity measurements. The model fits are compared to previously collected temperature dependent viscoelastic measurements on VHB 4905 for temperatures ranging from 23 °C to 60 °C. Based on fractional order viscoelasticity, we infer that the excluded volume parameter is negative and initially decreases before reaching a constant value near 50 °C.

1. Introduction

Fractals are self-replicating geometries that occur across all length or time scales (Mandelbrot et al., 2004). This mathematical construct provides a unique tool to understand complexities in mechanics of materials (West and Grigolini, 2010). In polymer science, this characteristic can manifest as monomers forming polymer networks that lead to complex multiscale structures from the network's topology, distributions of the crosslink density, free volume distributions, mesoscale phase distributions, etc. When these polymer structures form fractal geometries, their structure is difficult to represent on a Euclidean domain since length measures, and the associated displacement gradients, may not have finite values. This poses challenges in constructing accurate constitutive laws using common integer order calculus. When represented on a fractal domain; however, deformation and stress are expected to be better represented using fractal or fractional order derivatives (West et al., 2012; Li and Ostoja-Starzewski, 2009). We investigate this concept by validating a fractal inspired modeling using an information theoretic framework to construct a hyperelastic and viscoelastic model for temperature dependent, finite deformation in elastomers based on a set of experimental data.

Application of fractional order calculus to mechanics of materials has seen a resurgence in theoretical and computational developments (Tarasov, 2011; Lischke et al., 2020; Li and Ostoja-Starzewski, 2020; Mashayekhi et al., 2018, 2021; Pahari and Oates, 2022). This has stimulated further interest in probing complex multiscale structure of materials and relating these structures to fractional order operators within the constitutive models and balance laws (Wheatcraft and Meerschaert, 2008; Mashayekhi et al., 2019). The concept is different from conventional multiscale mechanics models that fuse different physical processes at the quantum, molecular, micro, meso, and macro scales (Tadmor and Miller, 2011). Fractals represent geometrical complexity which cannot easily be reduced down to elementary parts because of non-local interactions in space or time which propagate across scales in complex and unpredictable ways (West and Grigolini,

* Corresponding author.
E-mail addresses: els18u@my.fsu.edu (E. Stanisauskis), smashay1@kennesaw.edu (S. Mashayekhi), bpahari@eng.fsu.famu.edu (B. Pahari), markus.mehnert@fau.de (M. Mehnert), paul.steinmann@fau.de (P. Steinmann), woates@fsu.edu (W. Oates).

https://doi.org/10.1016/j.mechmat.2022.104390
Received 30 January 2022; Received in revised form 18 May 2022; Accepted 3 June 2022
Available online 17 June 2022

2010). Fractional order operators are often better suited to handle such behavior; however, appropriate connections between fractal geometry and fractional property relations remain a challenge. It is often argued that given a fractal geometry, heat, stress, chemical diffusion, etc. diffuses across the material while constrained to a random walk on a fractal domain Havlin and Ben-Avraham (1987), Balankin (2015). Recent results have applied this concept to fractional viscoelasticity (Mashayekhi et al., 2019). This prior work on viscoelasticity did not consider temperature dependent constitutive behavior. In this work, we explore how the fractal and fractional order model assumptions provide insight into simulating viscoelasticity on an elastomer deformed at constant temperatures ranging from room temperature up to 60 °C.

More broadly, development of constitutive relations and balance equations of momentum, energy, and entropy rely on Taylor expansions and integrals that are localized to a continuum point. Whether it is derivatives associated with a Taylor expansion or spatial or time derivatives from the divergence or Reynold's transport theorem, integer derivatives are routinely used (Malvern, 1969). Under certain restrictions of power-law relations, fractional derivatives have shown to be superior in predicting behavior farther away from operating points along a Taylor series (Wheatcraft and Meerschaert, 2008). These power-law characteristics, such as fluid flow or heat through complex media, are often motivated by the presence of fractal media. The connections between a fractal solid and a *fractional* operator that describes constitutive behavior remains elusive. The fractal structure of a solid can be well described using the Hausdorff dimension which can be estimated accurately using the box-counting method (Falconer, 2004). However, fractional operators are used to predict stress from deformation and deformation rates that may follow some fractal path (i.e., a power-law function). The direct mapping of fractal structure to fractional properties remains an open question. There are further questions about the distinctions between fractional order (non-local) operators (Tarasov, 2005) versus fractal order (local) operators (Chen et al., 2017) that may both provide good predictions of stress and transport phenomena in fractal media. Given these challenges, we approach the problem here using an information theoretic framework to elucidate the origin of assumptions so that further developments can be made to build better models, via integer, fractional, or fractal order operators, to better predict constitutive behavior in materials that exhibit fractal structure. We adopt methods from entropy dynamics (Caticha, 2015) which combines Shannon's entropy with fractional order constraints on material kinematics (integer operators are the limiting case). This includes a fractional covariance matrix that provides partial information to inform the model to enhance prediction. This may come from experiments or higher fidelity models. We use this information to guide the form of the spatial and temporal derivative operators used in constructing the viscoelastic constitutive equations.

Previous work has shown a strong correlation between the order of the fractional derivative in the linear fractional model of viscoelasticity with fractal structure and excluded volume effects (Mashayekhi et al., 2021). The excluded volume measure is a well known concept used in polymer physics to describe the affinity between monomer chains within a bulk polymer. It is based on the Meyer function where the Boltzmann distribution is used to evaluate the probability of locating a monomer at the point r relative to the non-interacting case where the potential energy is zero ($U(r) = 0$). The Meyer function is mathematically represented by $f(r) = e^{-\frac{U(r)}{kT}} - 1$ where k is the Boltzmann constant and T is absolute temperature. The excluded volume is then represented by an integral over a representative material volume

$$\kappa = -\int 4\pi r^2 f(r) dr \tag{1}$$

and κ is positive for polymers with net repulsion between the monomers and negative for polymers with net attraction between the monomers (Rubinstein et al., 2003). This parameter influences the statistical properties of the polymer network including viscoelasticity. The work presented here will explore connections between the excluded volume and fractional viscoelasticity which builds off of prior theoretical analysis (Mashayekhi et al., 2021).

We explore temperature dependent hyperelastic and viscoelastic behavior by constructing a constitutive model using entropy dynamics (Caticha, 2015; Caticha and Preuss, 2004) to infer information about fractal and fractional order structure–property relations. A key distinction from prior entropy dynamics and the proposed framework is the use of fractional order constraints that lead to non-Gaussian Bayesian posterior densities. The form of these densities offer guidance to the proper fractional order derivative operators in the constitutive equations and the form of the free energy function. This provides a framework to understand connections between fractal structure and fractional deformation in elastomers. A hyperelastic model is obtained by maximizing Shannon's relative entropy under a power-law constraint of relative polymer network displacements. The power-law constraint is chosen given its characteristics associated with fractal geometry. We chose a fractal deformation gradient to represent the kinematics based on arguments given in Appendix. This kinematic assumption and hyperelastic model are combined with fractional order viscoelasticity to accommodate hysteresis as a function of stretch rate. Prior fractional order viscoelasticity (Mashayekhi et al., 2019) is extended to assess assumptions associated with fractional excluded volume behavior to evaluate a recent theoretical relation (Mashayekhi et al., 2021). This is achieved through model comparisons of experimental viscoelastic measurements in the elastomer made by 3M (Very High Bond (VHB) 4905) as a function of temperature from 23°C to 60 °C (Mehnert et al., 2021). The inference and uncertainty of the fractal excluded volume are quantified across this temperature range using Bayesian statistics.

In Section 2, we briefly describe the theory for fractal hyperelasticity and fractional order viscoelasticity. In Section 3, we validate the model on VHB 4905 across a range of temperatures and quantify changes in the fractal excluded volume relative to the fractional viscoelastic order. The change in viscoelasticity from room temperature to 60 °C is used to estimate how the excluded volume changes as a function of temperature. Concluding remarks are given in the final section.

2. Theoretical approach

Since limited knowledge is available about the chemical structure of the commercial VHB elastomer, we infer structure–property relations from temperature dependent stress measurements at a fixed strain rate (Mehnert et al., 2021). We apply an information theoretic approach to derive stress–stretch behavior as a function of random particle motion assuming the polymer network's motion is constrained to fractal geometry. This allows us to explore power-law constraints for both observable and non-observable (internal state) material displacements that contribute to reversible and irreversible deformation. The methodology starts with Shannon's relative entropy which is maximized subject to a set of fractional constraints that penalize relative particle displacements, presumably along a fractal polymer network. Constitutive relations for hyperelastic and viscoelastic stress over a range of temperatures are formulated from the Bayesian posterior density that are derived from maximizing Shannon's entropy under fractional deformation constraints.

The relative fractal displacements are based on a dimensional regularization of the true Euclidean domain displacements. This provides a means to homogenize and approximate multiscale displacement measures as a finite measure based on the constraint of fractal geometry. Importantly, this assumption involves relating fractal structure, which may be quantified via microscopy and box counting methods, with material displacements that are assumed to move along the fractal geometric constraints. We use a density of state to regularize displacements

that are assumed to follow a fractal pattern. Details of the isotropic density of state are given by Tarasov (2011) and the anisotropic density of state is given by Li and Ostoja-Starzewski (2009). In the present model, we assume isotropic densities of state and spherical symmetry. We avoid the need for micropolar theory and asymmetric Cauchy stresses, as described elsewhere (Li and Ostoja-Starzewski, 2009), through the use of homogenization over a characteristic length scale. More details discussing this homogenization, the fractal deformation gradient, and associated invariance relations are given in Appendix.

2.1. Entropy dynamic method

We introduce a fractal measure of geometry to estimate complex deformation in elastomers. This approach uses a power-law relation to quantify length measures between the fractal domain and the Euclidean domain. By focusing on isotropic fractals (Tarasov, 2011), we define a relative fractal displacement as

$$\Delta\mu_i(x_i,t) = \mu_i(x_i+\Delta x_i,t) - \mu_i(x_i,t) = c_1^{(i)}(\nu,x_i)\Delta x_i(X_K,t) \tag{2}$$

where $c_1^{(i)}$ is the isotropic density of state along the Euclidean direction of the relative distance between particles in the deformed (Eulerian) frame Δx_i where we have $\Delta x_i(X_K,t) = x_i(X_K+\Delta X_K,t) - x_i(X_K,t)$ and X_K is the Lagrangian coordinate (Malvern, 1969) (no sum on i in the density of state). The isotropic fractal dimension is given by ν and ranges between 0 and 1. Several forms of the line transformation have been considered and have different trade-offs (Li and Ostoja-Starzewski, 2020), but they generally include a power-law dependence on the Euclidean coordinates x_i. The isotropic density of state and methods used here to obtain a fractal deformation gradient are further described in the subsequent paragraphs.

The changes in fractal displacements of neighboring points separated over the Euclidean frame (Δx_i) are expected to be well approximated using a fractal Taylor expansion to first order

$$\mu_i(x_i+\Delta x_i,t) \simeq \mu_i(x_i,t) + \frac{\partial\mu_i}{\partial x_i^\beta}[x_i^\beta - (x_i')^\beta]. \tag{3}$$

In the Appendix, we use the chain rule between the Eulerian coordinates x_i and the Lagrangian coordinates X_K to obtain a definition for fractal displacements in terms of the fractal deformation gradient of order $\beta > 0$ as

$$d\mu_i = \frac{\partial\mu_i}{\partial X_K^\beta} dX_K = F_{iK}^\beta dX_K. \tag{4}$$

Here we have taken the limit $\Delta x_i \to dx_i$, $\Delta X_K \to dX_K$, and $\Delta\mu_i \to d\mu_i$. In the limiting case of $\beta = 1$, we obtain the conventional definition of the deformation gradient describing material deformation of a continuum volume element relative to its undeformed configuration (Malvern, 1969). Furthermore, in the case of $\nu = 1$ from (2) and consequently, $c_1^{(i)} = 1$, we have $\Delta\mu_i = \Delta x_i$. The fractal deformation gradient is used to better estimate material deformation of particle motion that is expected to follow power-law (fractal) behavior. We also note that β should be equivalent to ν in the density of state if deformation follows the fractal dimension in the undeformed Lagrangian configuration. We let these parameters be different initially to highlight places where uncertainty can occur once the chain rule is applied to obtain the fractal deformation gradient. This is described in more detail in Appendix.

The fractal measure $\boldsymbol{\mu}$ is broken down into an observable ($\boldsymbol{\mu}_1$) and a non-observable ($\boldsymbol{\mu}_2$) vector to accommodate reversible and irreversible (viscoelastic) deformation. The total set of fractal displacement measures is denoted by $\boldsymbol{\mu} = [\boldsymbol{\mu}_1, \boldsymbol{\mu}_2]$ which results in a 6×6 size deformation gradient to accommodate both observable and non-observable deformations. This results in a block diagonal matrix form where F_{iK}^β contains the conventional 3×3 deformation gradient $\mathbf{F}^{\beta(1)} = \frac{\partial\boldsymbol{\mu}_1}{\partial\mathbf{X}}$ and $\mathbf{F}^{\beta(2)} = \frac{\partial\boldsymbol{\mu}_2}{\partial\mathbf{X}}$. The 6×6 deformation gradient is written in terms of the observable and non-observable 3×3 matrices as

$$\mathbf{F}^\beta = \begin{bmatrix} \mathbf{F}^{\beta(1)} & \mathbf{0} \\ \mathbf{0} & \mathbf{F}^{\beta(2)} \end{bmatrix} \tag{5}$$

where $\mathbf{0}$ is a 3×3 matrix of zeros.

We use this fractal deformation gradient to model stresses during viscoelastic finite deformation. For more details on the fractal derivative operator applied in fractal mechanics, see Li and Ostoja-Starzewski (2013). It is important to note that translational and rotational invariance of the fractal metric has been discussed by Tarasov (Tarasov, 2011) which only holds over the entire fractal set. This poses challenges when taking limits to a point as is typically done in continuum mechanics. Details discussing how we address the invariance problem are given in Appendix.

These measures of fractal displacements are integrated into an entropy dynamics framework to formulate a free energy function from information theory that is connected to thermodynamic entropy. We combine Shannon's relative entropy with a fractional constraint on the fractal relative displacements in (2). More details on the optimization of the cost function containing Shannon's entropy and the fractional order constraint can be found elsewhere (Oates et al., 2021). Key details are given as follows.

The cost function that is used to obtain the Bayesian posterior density is

$$\begin{aligned} H[P,Q] = S[P,Q] &- \gamma\left(\int_D P(\boldsymbol{\mu}|\mathbf{X})d\boldsymbol{\mu} - 1\right) \\ &- \mathrm{Tr}\left\{\boldsymbol{\Lambda}\cdot\left(\int_D P(\boldsymbol{\mu}|\mathbf{X})\mathbf{C}_X^{\frac{\nu}{2}}d\boldsymbol{\mu} - \boldsymbol{\Sigma}^{\frac{\nu}{2}}(t)\right)\right\}. \end{aligned} \tag{6}$$

In this equation, the posterior probability $P(\boldsymbol{\mu}|\mathbf{X})$ quantifies the conditional probability of having the fractal configuration $\boldsymbol{\mu}$ given $\mathbf{X}$. This amounts to a probabilistic model that gives estimates of the possible fractal displacements given an undeformed (Lagrangian) material configuration. In the cost function defined here, two constraints have been introduced. The first constraint restricts the probability $P(\boldsymbol{\mu}|\mathbf{X})$ to integrate to one over all possible $\boldsymbol{\mu}$ configurations that is penalized by the Lagrange multiplier γ. The second constraint imposes a fractional penalty on relative particle motion which we denote by the tensor product, $\mathbf{C}_X^{\nu/2} = (\Delta\boldsymbol{\mu}\Delta\boldsymbol{\mu})^{\nu/2}$, to follow the time-dependent fractional covariance matrix $\boldsymbol{\Sigma}^{\nu/2}(t)$. This integral is penalized by the Lagrangian matrix $\boldsymbol{\Lambda}$. Again, these relative fractal displacements are broken into observable ($\Delta\boldsymbol{\mu}_1$) and non-observable ($\Delta\boldsymbol{\mu}_2$) internal state displacements. More details about these terms are given in subsequent paragraphs.

The two constraints in (6) are balanced by the relative Shannon entropy, $S[P,Q]$. It is defined in terms of the Bayesian posterior P and a prior density Q that is given by

$$S[P,Q] = -\int_D P(\boldsymbol{\mu}|\mathbf{X})\ln\left(\frac{P(\boldsymbol{\mu}|\mathbf{X})}{Q(\boldsymbol{\mu}|\mathbf{X})}\right)d\boldsymbol{\mu} \tag{7}$$

which gives a measure of the distance between the posterior P and the prior Q densities. The prior density is generally defined as a conditional probability of the form $Q = Q(\boldsymbol{\mu}|\mathbf{X})$. These two probabilities of the fractal displacements are conditioned upon the undeformed material points $\mathbf{X}$.

In (6), we have divided changes in the fractal displacement into observable $\Delta\boldsymbol{\mu}_1$ and non-observable $\Delta\boldsymbol{\mu}_2$ terms which comprise the complete measure $\boldsymbol{\mu} = [\boldsymbol{\mu}_1, \boldsymbol{\mu}_2]$ that is contained in $P(\boldsymbol{\mu}|\mathbf{X})$ and $Q(\boldsymbol{\mu}|\mathbf{X})$ for brevity. If all displacements are observable, the deformed fractal positions $\boldsymbol{\mu}$ share similarities with the Eulerian frame (deformed) material points, $\mathbf{x}(\mathbf{X},t)$ (Malvern, 1969; Sumelka, 2014; Tarasov, 2011). The non-observable fractal displacements contribute to the entropy generation and viscoelastic stresses. We will illustrate how the viscoelastic effects manifest from time dependence in the covariance matrices given by $\boldsymbol{\Sigma}(t)$.

The second and third terms in (6) include the probability normalization constraint and the fractional displacement constraint in the second

and third terms, respectively. These constraints are enforced by the scalar Lagrange multiplier γ and the Lagrange multiplier matrix $\boldsymbol{\Lambda}$. The latter is a 6×6 matrix given that $\boldsymbol{\mu} = [\boldsymbol{\mu}_1, \boldsymbol{\mu}_2]$ consist of two 3×1 vectors or a single 6×1 vector. The fractional order covariance matrix ($\boldsymbol{\Sigma}^{\frac{\nu}{2}}$) is similarly defined by a 6×6 matrix. This matrix is raised to a power using conventional operations by rotating the tensors to their eigendirections, applying the exponents to the eigenvalues, and rotating the tensors back to their original directions. The covariance matrix is positive semi-definite and symmetric which results in real valued components after being raised to the positive fractional power $\nu/2$. From a physical perspective, this fractional power penalizes fractal displacements relative to their initial positions by assuming future displacements follow a power-law displacement function that is constrained by the original fractal structure of the material. In the limiting case of $\nu = 2$, a Gaussian network is obtained which results in the conventional neo-Hookean model (Weiner, 2012). It is possible that this exponent is dependent upon the original fractal structure in some complicated way (Havlin and Ben-Avraham, 1987). Here we assume they are equal and properties are inferred using the cost function, experimental data and Bayesian uncertainty analysis.

The resulting Bayesian posterior density is obtained from maximizing the cost function in (6) which gives a stretched exponential posterior density (Oates et al., 2021). We use this posterior as the starting point to construct the constitutive model for rate dependent elastomer deformation according to

$$P(\boldsymbol{\mu}|\mathbf{X}) = Z^{-1} e^{-\operatorname{Tr}\left(\hat{\boldsymbol{\Lambda}}^{-\nu/2} \cdot \mathbf{D}_X^{\nu/2}\right)} \tag{8}$$

where Z is a partition function that ensures integration of the posterior density equals one based on solving for the Lagrange multiplier γ via the first constraint in (6); see Caticha (2015) for details. The rotated Lagrange multiplier matrix is denoted by $\hat{\boldsymbol{\Lambda}}$ and it is assumed that $\mathbf{C}_X$ has the same eigendirections as $\boldsymbol{\Lambda}$. The matrices $\mathbf{D}_X$ and $\hat{\boldsymbol{\Sigma}}$ are diagonalized matrices with eigenvalues as diagonal entries of $\mathbf{C}_X$ and $\boldsymbol{\Sigma}$ respectively. The form of the posterior density given in terms of the fractional covariance matrix and fractal exponent ν is eventually

$$P(\boldsymbol{\mu}|\mathbf{X}) = \frac{\nu^6 M^{6/\nu}}{2^6 (\Gamma(\nu^{-1}))^6} \det\left(\boldsymbol{\Sigma}^{-\nu/2}\right)^{1/\nu} e^{-M \operatorname{Tr}\left(\boldsymbol{\Sigma}^{-\nu/2}(t) \cdot \boldsymbol{C}_{\mathbf{X}}{}^{\nu/2}\right)}. \tag{9}$$

where we let $M = \frac{\Gamma(\frac{\nu+1}{\nu})}{\Gamma(\nu^{-1})}$ and $\Gamma(\cdot)$ is the Gamma function. This expression gives a conditional probability for the new fractal relative positions. We take the limit: $\Delta\boldsymbol{\mu} \to d\boldsymbol{\mu}$ such that $\mathbf{C}_X^{\nu/2} = (d\boldsymbol{\mu} d\boldsymbol{\mu})^{\nu/2}$. The parameter ν originates in the fractional order penalties on $\Delta\mu_i$ (Oates et al., 2021) with $\nu = 2$ giving the limit of a Gaussian process. If $\nu < 2$, the posterior is a stretched exponential in terms of the relative fractal displacements.

A substitution of the fractal deformation gradient based on (4) into (9) gives

$$P(\boldsymbol{\mu}|\mathbf{X}) = \frac{\nu^6 M^{6/\nu}}{2^6 (\Gamma(\nu^{-1}))^6} \det\left(\boldsymbol{\Sigma}^{-\nu/2}\right)^{1/\nu} e^{-M \operatorname{Tr}\left(\boldsymbol{\Sigma}^{-\nu/2}(t) \cdot [(\mathbf{F}^{\nu} \cdot d\mathbf{X})(\mathbf{F}^{\nu} \cdot d\mathbf{X})]^{\nu/2}\right)}. \tag{10}$$

This final expression relates the Euclidean frame deformation gradient to an approximation of the fractal deformation gradient given by

$$d\mu_i = F_{iK}^{\nu} dX_K = \frac{\pi^{\nu/2}}{2^{\nu-1} l_0 \Gamma(\nu/2)} F_{iK} dX_K \tag{11}$$

where $\Gamma(\nu/2)$ is again the Gamma function and we have introduced a characteristic length scale l_0. Unlike in the Appendix where we assume uncertainty in the knowledge of ν, we have assumed the fractal dimension is exactly known here such that $F_{iK}^{\beta} = F_{iK}^{\nu}$ where $\beta = \nu$ as previously described by (2) and (3); see the Appendix for further details.

From the Bayesian posterior density in (10), we formulate a free energy function to quantify the reversible stress. This first requires defining a thermodynamic entropy from the Bayesian posterior density. A comparison of the Gibbs and Boltzmann entropy functions has been described by Jaynes (1965). It was shown that the Gibbs function accommodates interactions among neighboring particles while the Boltzmann function neglects interactions. The Gibbs function is equivalent to the Shannon entropy used here excluding the prior density. Further, simplifications of the Gibbs or Shannon entropy function can be made if the entropy quantifies the phase volume of 'reasonably probable' events (Jaynes, 1965). This simplified thermodynamic entropy function is given directly by $S = -k \ln(P)$. In comparison, it neglects the averaging over all probability states, i.e., $S = -k \int P \ln(P) dV$. Given that our probability is defined for a dimensionally regularized fractal displacement measure by homogenizing $\boldsymbol{\mu}$ over a characteristic length scale l_0, we also assume 'reasonably probable' events via this dimensional regularization given by the densities of state power-law relation in $c_1^{(k)}$ and the relations in Appendix.

Given these arguments, we define the total entropy of the material to be

$$S_T = -k \ln P(\boldsymbol{\mu}|\mathbf{X}) \tag{12}$$

which includes both reversible and irreversible effects. The reversible effects are contained within the measure $\boldsymbol{\mu}_1$ and the irreversibilities are contained within $\boldsymbol{\mu}_2$. These separate effects have been lumped into the Bayesian posterior (10).

The reversible and irreversible components contained within S_T are separated based on time invariant and time dependent terms in the covariance matrix $\boldsymbol{\Sigma}(t)^{-\nu/2} = \overline{\boldsymbol{\Sigma}}^{-\nu/2} + \delta\boldsymbol{\Sigma}(t)^{-\nu/2}$ where $\overline{\boldsymbol{\Sigma}}^{-\nu/2}$ is the fractional time invariant covariance and $\delta\boldsymbol{\Sigma}(t)^{-\nu/2}$ is the time varying fractional covariance. These two components are written in terms of the functions

$$\begin{aligned} \overline{\boldsymbol{\Phi}} &= -M \operatorname{Tr}\left(\overline{\boldsymbol{\Sigma}}^{-\nu/2} \cdot \mathbf{C}_X^{\nu/2}\right) \\ \boldsymbol{\Phi}_t &= -M \operatorname{Tr}\left(\delta\boldsymbol{\Sigma}(t)^{-\nu/2} \cdot \mathbf{C}_X^{\nu/2}\right) \end{aligned} \tag{13}$$

where $\overline{\boldsymbol{\Phi}}$ is the time invariant component and $\boldsymbol{\Phi}_t$ is the time varying component. We can now re-write the entropy function as

$$S_T = -k\left(\ln(Z) + \overline{\boldsymbol{\Phi}} + \boldsymbol{\Phi}_t\right) \tag{14}$$

where $Z = \frac{\nu^6}{2^6(\Gamma(\nu^{-1}))^6}\left(\frac{\Gamma(\frac{\nu+1}{\nu})}{\Gamma(\nu^{-1})}\right)^{6/\nu} \det\left(\boldsymbol{\Sigma}^{-\nu/2}\right)^{1/\nu}$ from (10).

We further simplify the deformation gradient into its principle stretch components using λ_j as the principle stretch components for F_{iK}^{ν}. Recall that our definition of the deformation gradient includes observable and non-observable components. This requires us to include three observable stretches λ_j for $j = 1, 2, 3$ and three non-observable stretches for $j = 4, 5, 6$. We can now write the time invariant expression for $\overline{\boldsymbol{\Phi}}$ as

$$\overline{\boldsymbol{\Phi}} = -M A_0 \sum_{k=1}^{6} \sum_{l=1}^{6} \overline{\Sigma}_{kl}^{-\nu/2} (\lambda_k \lambda_l)^{\nu/2} \tag{15}$$

where we include the explicit summation over the observable and non-observable stretch ratios and $A_0 = (dX_I dX_I)^{\nu/2}$. An analogous expression can be written for $\boldsymbol{\Phi}_t$ using $\delta\boldsymbol{\Sigma}(t)$.

In the following subsection, we take this time invariant portion of the entropy in (14) and formulate a free energy expression followed by the hyperelastic stress relations. The portion of the entropy that contains time varying behavior (e.g, within $\boldsymbol{\Phi}_t$), is then used to formulate the entropy generation and viscoelastic stresses associated with non-measurable deformation contained within the fractal stretch $\lambda_{Q(2)}^{\nu}$.

2.2. Constitutive relations

We first define the free energy density using the reversible part of the entropy function (14) as $\psi = -TS_{T,0}$ where T is the absolute temperature and $S_{T,0} = -k(\ln(Z) + \overline{\boldsymbol{\Phi}})$ neglects contributions from $\boldsymbol{\Phi}_t$

and internal energy. We lump the parameters from (15) together and assume certain symmetry on the covariance matrix $\overline{\Sigma}_{kl}^{-\nu/2}$. We assume 3×3 block diagonal form requiring three phenomenological constants: one parameter governing observable stretch (f_0^{11}), one governing non-observable stretch (f_0^{12}), and one coupling term (f_0^{22}). This can be written as

$$\psi = T\left[\sum_{Q=1}^{3}\left(f_0^{11}\lambda_Q^\nu + 2f_0^{12}(\lambda_Q\lambda_{Q+3})^{\nu/2} + f_0^{22}(\lambda_{Q+3}^\nu)\right)\right] \tag{16}$$

where the phenomenological parameters f_0^{11}, f_0^{12} and f_0^{22} contain $kM\overline{\Sigma}_0^{AB}A_0^{\nu/2}$. Also note that we are defining the observable stretches for λ_Q for $Q = 1,2,3$ and λ_{Q+3} for $Q = 4,5,6$. This function therefore has three unknown constitutive parameters plus the fractional order parameter ν. We have neglected the constant associated with the partition function Z since it does not influence the stress.

We add an incompressibility constraint into this free energy function to accommodate elastomer deformation that occurs over a constant volume process. This involves the additional free energy component

$$\hat{\psi} = \psi - p_h[J^\nu - 1] \tag{17}$$

where $J^\nu = \lambda_1^\nu\lambda_2^\nu\lambda_3^\nu$ and p_h is an unknown hydrostatic pressure that is multiplied by $J^\nu - 1$ to constrain the volume to be incompressible. The total stress is defined by changes in the free energy with respect to the observable stretch ratio

$$s_L^{tot} = \frac{\partial\hat{\psi}}{\partial\lambda_L^\nu} = T\left[\nu f_0^{11}(\lambda_Q^\nu\lambda_Q^\nu)^{\nu/2-1}\lambda_L^\nu + \nu f_0^{12}(\lambda_Q^\nu\lambda_{Q+3}^\nu)^{\nu/2-1}\lambda_{L+3}^\nu\right] - p_h\frac{\partial J^\nu}{\partial\lambda_L^\nu}. \tag{18}$$

By defining $I_1^{11} = \lambda_Q^\nu\lambda_Q^\nu$, $I_1^{12} = \lambda_Q^\nu\lambda_{Q+3}^\nu$, and $I_1^{22} = \lambda_{Q+3}^\nu\lambda_{Q+3}^\nu$ we can re-write the stress as

$$s_L^{tot} = T\nu\left[f_0^{11}(I_1^{11})^{\nu/2-1}\lambda_L^\nu + f_0^{12}(I_1^{12})^{\nu/2-1}\lambda_{L+3}^\nu\right] - p_h\frac{\partial J^\nu}{\partial\lambda_L^\nu}. \tag{19}$$

We highlight here the identifiability of ν due to its reliance as an exponent of the invariants as well as the first term in the equation above since it gives some indication of fractal structure from material property relations. We now focus on uniaxial loading which allows the hydrostatic pressure to be found in closed form. This pressure is found by applying the zero transverse stress constraint for uniaxial loading applied in the 3-direction, which gives

$$p_h = \frac{T\nu\left[f_0^{11}(I_1^{11})^{\nu/2-1}\lambda_1^\nu + f_0^{12}(I_1^{12})^{\nu/2-1}\lambda_1^\nu\right]}{\lambda_2^\nu\lambda_3^\nu}. \tag{20}$$

This takes the 1 and 2 directions to be the zero transverse stress directions.

The observable fractal stretch, λ_L^ν, is related to the stretch in the Euclidean domain using the transformation (41) given in Appendix. A scaling relationship between the fractal domain and the Euclidean domain gives

$$\lambda_L^\nu = \frac{\pi^{\nu/2}}{2^{\nu-1}l_0\Gamma(\nu/2)}\lambda_L \tag{21}$$

where l_0 is the characteristic length scale. This relation allows for the observable stretch (λ_L) to be related to the fractal stretch (λ_L^ν) that is used in the stress–stretch constitutive relation given by (19).

2.3. Entropy generation and viscoelasticity

The implementation of fractional viscoelasticity follows the thermodynamic framework previously described elsewhere (Mashayekhi et al., 2018). This method follows the conventional approach of combining the first and second laws of thermodynamics, except the time rates of change are presumed to be better described by fractional time derivatives. We relate these balance equations with the information theoretic approach used here. This requires relating the entropy function (14) to an entropy generation function that is used to describe irreversible viscoelastic stress.

Under the assumption of negligible temperature gradients and fractional rates of change of the internal state variables, combining the first and second laws of thermodynamics results in the inequality (Mashayekhi et al., 2018),

$$S_g = -\frac{\partial\hat{\psi}}{\partial F_{iK(2)}^\nu}D_t^\alpha F_{iK(2)}^\nu(t) = Q_{iK}D_t^\alpha F_{iK(2)}^\nu(t) \geq 0 \tag{22}$$

where S_g is the entropy generation and irreversibilities are contained in the viscoelastic stress relation $Q_{iK} = -\frac{\partial\psi}{\partial F_{iK(2)}^\nu}$. We have denoted $F_{iK(2)}$ as the non-observable components of the deformation gradient $\mathbf{F}^{\nu(2)} = \mathbf{F}^{\beta(2)}$ given in (5). Based on the assumed power-law relation in the fractal kinematic relations, we have assumed that rates of deformation are better approximated by fractional time derivatives on the fractal deformation gradient of the Caputo form, D_t^α, which is defined by

$$D_t^\alpha F_{iK(2)}^\nu(t) = \frac{1}{\Gamma(n-\alpha)}\int_0^t \frac{F_{iK(2)}^{\nu(n)}(s)}{[t-s]^{\alpha+1-n}}ds \tag{23}$$

for $n-1 < \alpha \leq n$, $n \in \mathbb{N}$

where $\alpha > 0$ is the fractional order of the time derivative and n is the smallest integer greater than α. This fractional order α is connected to the fractal structure dimension ν based on certain assumptions of random walks on a fractal domain Mashayekhi et al. (2018). We give further details on fractal structure–fractional order time rates in Section 2.4. The integer time derivative of the deformation gradient is given by $F_{iK(2)}^{\nu(n)}$ where we focus on the case of first order time derivatives with $n = 1$. We note that several fractional order operators or fractal operators (Chen et al., 2010) could be used to estimate the viscoelastic behavior. For example, the Riemann-Liouville fractional order operator could be used; however, it gives a non-zero value for a constant. Local fractal operators may also be considered which share certain similarities with fractional order operators that are beyond the scope of the present work. We focus on the use of fractional order Caputo derivatives here to build upon prior theoretical analysis (Mashayekhi et al., 2021) that used fractional order excluded volume effects. The relation given by (22) defines the governing equation to solve for the irreversible deformation gradient components. Recall the entropy S_T contains a time varying component in Φ_t that leads to the entropy generation function S_g. In our model, this time varying property is based on the assumption of a time varying covariance matrices, $\delta\boldsymbol{\Sigma}(t)$. Classical diffusion processes assume the covariance matrix scales linear in time. For example, the variance that describes the distribution of localized heat spreads out linear in time as a Gaussian distribution for ideal (non-fractal) materials. In the case of fractal media, material complexities may slow the spread of heat or other irreversibilities (local residual strains, non-modeled molecular degrees of freedom) which may diffuse proportional to t^α where $0 \leq \alpha \leq 1$. As such, we assume $\delta\boldsymbol{\Sigma}(t) \propto t^\alpha$. This motivates the application of the fractional derivative in (23) since it has been shown that first order fractional Taylor series approximations of power-law functions are exact (Wheatcraft and Meerschaert, 2008).

We choose a quadratic function for S_g in terms of the fractional time derivative of the non-observable (internal state) deformation $F_{iK(2)}^\nu$ to ensure the entropy generation function is positive definite. In this case, we have

$$S_g = \eta_\alpha D_t^\alpha F_{iK(2)}^\nu D_t^\alpha F_{iK(2)}^\nu \tag{24}$$

where $\eta_\alpha > 0$ is a dissipative viscous parameter. When this function is written in terms of the stretch ratio, we have $S_g = \eta_\alpha D_t^\alpha\lambda_{L+3}^\nu D_t^\alpha\lambda_{L+3}^\nu$ where we have again denoted the non-observable stretch ratios by λ_{L+3} for $L = 1,2,3$.

Substitution of (24) into (22) gives the general viscoelastic stress equation

$$\eta_\alpha D_t^\alpha F_{iK(2)}^\nu(t) = Q_{iK}. \tag{25}$$

We now write this expression in terms of the principle stretch components. For uniaxial problems where $L = 3$ is again the loading direction, the viscoelastic stress is

$$Q_3 = -T\nu\left[f_0^{12}(I_1^{12})^{\nu/2-1}\lambda_3^{\nu} + f_0^{22}(I_1^{22})^{\nu/2-1}\lambda_6^{\nu}\right] \tag{26}$$

and the viscoelastic equation is given by

$$\eta_\alpha D_t^\alpha \lambda_6^{\nu} + T\nu f_0^{22}(I_1^{22})^{\nu/2-1}\lambda_6^{\nu} = -T\nu f_0^{12}(I_1^{12})^{\nu/2-1}\lambda_3^{\nu}. \tag{27}$$

It should be noted that in the limit of Gaussian behavior (i.e., neo-Hookean behavior), the time constant of this model becomes $\tau_\alpha = \frac{\eta_\alpha}{2Tf_0^{22}}$. In addition, an assumption is made that the viscoelastic stress is not affected by the hydrostatic pressure. To fully solve for the non-observable stretch in the loading direction, we assume the Jacobian for the non-observable stretch ratios is also incompressible: $J^{\nu(2)} = \lambda_4^{\nu}\lambda_5^{\nu}\lambda_6^{\nu} = 1$ which may introduce additional model-based uncertainty into the analysis.

2.4. Excluded volume relation

Prior work (Mashayekhi et al., 2021, 2019) defines a relation between the fractional viscoelastic order and the excluded volume effect that is derived from the Zimm polymer model. This relations leads to

$$\alpha = \frac{2d_s + d_s d_f}{2(2+\kappa)} \tag{28}$$

where d_s is the spectral dimension, d_f is the two dimensional fractal dimension, and κ is the excluded volume. The spectral dimension is proportional to a ratio of the fractal random walk dimension on a two dimensional plane and the fractal dimension. It can be identified through the power-law relation that regulates the amplitudes of vibrations across the frequency spectrum (Alexander and Orbach, 1982; Havlin and Ben-Avraham, 1987; Balankin et al., 2012) or experimentally from infrared measurements (Mashayekhi et al., 2019). The fractal dimension is related to the fractal structure of the material which can be characterized via optical analyses and the box-counting method (Miloevic et al., 2013).

In prior work (Mashayekhi et al., 2019), we quantified the spectral dimension, d_s, from transient infrared data on VHB 4910 and the two dimensional fractal dimension, d_f, from the microscopy images and the box-counting method. In the following section, we will investigate the additional effect of the excluded volume parameter by evaluating its estimated value from VHB viscoelastic data over a range of temperatures. We will assume the fractional viscoelastic order α and the excluded volume parameter κ are temperature dependent while d_s and d_f are constant over the temperature range tested. Hence, we will assume an inverse relationship between the fractional viscoelastic order and the excluded volume parameter as a function of temperature.

3. BayesIan uncertainty quantification

We use Bayesian uncertainty analysis to infer the hyperelastic and viscoelastic model parameters that include fractional order dissipation and the excluded volume parameter. Experimental results of temperature dependent viscoelasticity of VHB are used to validate the model (Mehnert et al., 2021). Stress versus stretch data at constant temperatures ranging from 23 °C to 60 °C containing 75 data points per data set were used to better understand changes in fractional viscoelastic order and the excluded volume.

The fractional order derivative is studied in this paper to describe the viscoelastic behavior of elastomers. Previous work studying the viscoelastic behavior of dielectric elastomers at room temperature can be found in Miles et al. (2015), Oates et al. (2018) and Mashayekhi et al. (2018). Temperature dependence is considered here by evaluating changes in hyperelastic and fractional order across the temperatures from 23 °C to 60 °C. The uncertainty quantification will be presented by first illustrating parameter identification and uncertainty followed by an error analysis of the calibrated models by comparisons to data and the uncertainty in estimating excluded volume effects.

3.1. Parameter estimation

Bayesian statistics are used to calibrate the parameters in both the hyperelastic and viscoelastic models. In order to calibrate the parameters, the model is compared with experimental data collected by Mehnert et al. (2021). The statistical model implemented is

$$s_3^{tot,data}(i) = s_3^{tot}(i;\theta) + \varepsilon(i), \qquad i = 1, \dots, N \tag{29}$$

where $s_3^{tot,data}(i)$ is the experimental stress measurements, $s_3^{tot}(i;\theta)$ is the model response, $\varepsilon(i)$ is the observation error of the model response, θ is a parameter set of random variable with underlying distributions, and N is the number of data points. The parameter distributions are quantified using Bayes' relation

$$\pi(\theta|s_3^{tot,data}) = \frac{p(s_3^{tot}|\theta)\pi_0(\theta)}{\int_{\mathbb{R}_p} p(s_3^{tot}|\theta)\pi_0(\theta)d\theta}. \tag{30}$$

The parameter distributions are developed through repeated sampling leading to posterior parameter densities ($\pi(\theta|s_3^{tot,data})$). The posterior parameter densities indicate the probability of the unknown parameters given the observed data. The densities are updated using the likelihood ($p(s_3^{tot}|\theta)$) of the model given a particular parameter set and any *a priori* knowledge that may constrain the parameters ($\pi_0(\theta)$). This prior density is assumed to have a flat distribution since no prior knowledge is know about the parameter distributions excluding positive definiteness of certain parameters. The denominator of Bayes' equation ensures the posterior distribution integrates to one. The likelihood function is defined as $p(s_3^{tot}|\theta) = e^{-\frac{SS}{2\sigma^2}}$ where SS is the sum-of-squares residual between the model and the data, $SS = \sum_{i=1}^{N}[s_3^{tot,data}(i) - s_3^{tot}(i;\theta)]^2$, and σ^2 is the unknown variance. The Markov Chain Monte Carlo (MCMC) sampling method is used in conjunction with the Delayed Rejection Adaptive Metropolis (DRAM) algorithm to develop the posterior distributions (Haario et al., 2001, 2006; Smith, 2013).

3.2. Model analysis

We begin by looking at the model composed of the hyperelastic and the fractional order viscoelastic parameters. MCMC and DRAM methods discussed in the above section are used to identify the parameters set in order to begin our analysis. We are therefore able to identify average values as well as probability distributions for each parameter in the parameter set

$$\theta = [\eta, \alpha, f_0^{11}, f_0^{12}, f_0^{22}, \nu] \tag{31}$$

where η and α relate to the fractional order viscoelastic behavior (see Eq. (25)) while f_0^{AB} and ν can be found in (18) and relate to the reversible behavior. Parameter chains from the MCMC analysis at 23°C can be seen in Fig. 1(a). Typically with Bayesian uncertainty quantification, a visual assessment is the most common and first test of convergence. For the parameter chain analysis, we observe the sampling history over a chosen amount of iterations. After 3×10^5 iterations, the chains look to have converged to a stable distribution. This is based on each chain appearing to have noise around a mean with no significant jumps or periods of stagnation. Details regarding the criteria for statistical acceptance and convergence tests when using DRAM can be found in Haario et al. (2006, 2001). If desired Gelman–Rubin and Geweke convergence diagnostics can be completed which test the final convergence state based on different initial starting points and the mean response of each parameter chain comparing the first 10% and the last 50%, respectively. However, these statistical diagnostics only prove that the chains have not 'not converged'. Values for these diagnostics can be found in Tables 1 and 2. The Geweke diagnostic values, which are derived from a standard Z-test, are all close to and below 1 proving the chains are stable. For the Gelman–Rubin diagnostic, a value of 1 would mean the chains are exactly the same. A large value suggests the variance can be decreased with

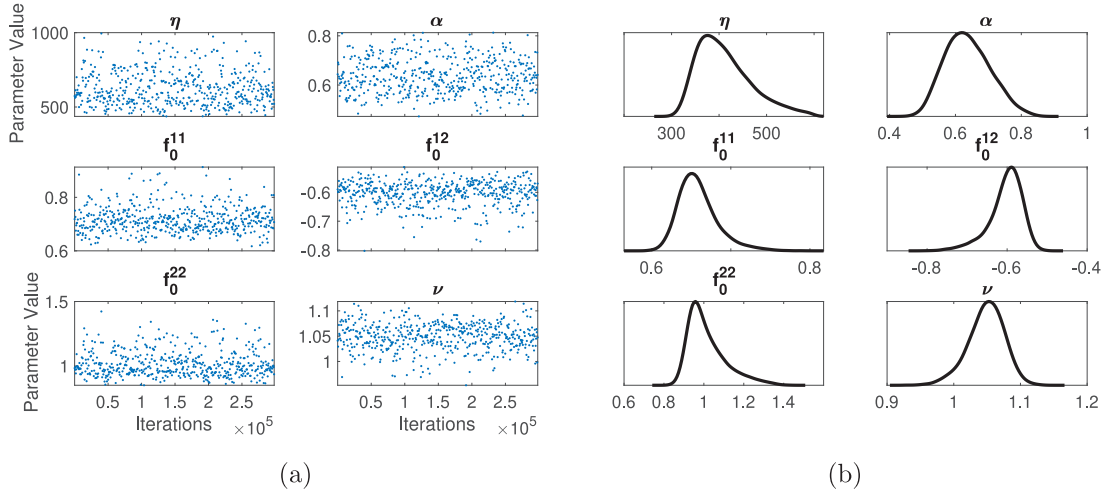

Fig. 1. Model parameter estimation results for T=23°C. (a) Parameter Chains. (b) Marginal posterior densities.

Table 1
Geweke convergence diagnostics.

Temperature (°C)	η	α	f_0^{11}	f_0^{12}	f_0^{22}	ν
23	0.998	0.999	0.999	0.999	0.999	0.999
30	0.996	0.996	0.992	0.993	0.995	0.997
40	0.998	0.999	0.997	0.998	0.998	0.999
50	0.993	0.979	0.959	0.963	0.974	0.983
60	0.998	0.998	0.995	0.996	0.998	0.998

Table 2
Gelman–Rubin convergence diagnostics.

Temperature (°C)	η	α	f_0^{11}	f_0^{12}	f_0^{22}	ν
23	1.00	1.03	1.02	1.01	1.01	1.03
30	0.999	1.06	1.13	1.12	1.08	1.10
40	1.01	0.996	0.993	0.999	0.990	0.993
50	1.01	0.997	0.992	1.01	0.992	0.999
60	0.997	1.01	1.03	1.01	1.01	1.01

more simulations. In general, there is no consensus of what the upper limit for this statistic should be though it must be close to one. For our purposes, a value less than 1.2 is deemed reasonable for this diagnostic. In Table 2, we see that the values are also very close to 1 meaning the variances are almost exactly the same no matter what the starting initial point is. The marginal posterior densities are then created from the converged parameter chains with the use of a kernel density estimator algorithm (Smith, 2013), see Fig. 1(b), to visualize the parameter distributions. The posterior densities for most parameters look to be of a nominal Gaussian distribution with some parameters having a thicker tail and asymmetry.

Another component of the analysis is the pairwise plot. This plots the parameter chains against each other to evaluate whether there are any correlations between the parameter pairs. The pairwise plot can be found in Fig. 2. Potential linear correlations can be see in the pairwise plot between (f_0^{11}, ν) suggesting there may be a simplified parameter set. A nearly linear relationship indicates that the parameter pairs may not be uniquely identifiable meaning that one can be functionally determined from the other. A rigorous assessment of the material physics may lead to model reduction, but for now we simply are aware that a correlation might exist and will interpret our results in light of that uncertainty. The scaling relationship in (21) is not directly identifiable since it is lumped into the constitutive parameters f_0^{11}, f_0^{12}, and f_0^{22}

Similar procedures are completed to calibrate the model parameters at all tested temperatures. We identify parameters for each temperature to identify sensitivity of the hyperelastic and viscoelastic parameters over the temperature range tested. The MCMC DRAM generated parameter chains for other temperatures were similar to the room temperature results shown in Fig. 1. Average parameter values and standard deviations for each calibrated parameter and temperature can be found in Tables 3 and 4, respectively. Relatively small fluctuations in the hyperelastic parameters were observed as a function of temperature with no obvious trend. Conversely, a reduction in the average viscous coefficient $\bar{\eta}$ was seen as the temperature increased as expected. We also observe that the fractional order of viscoelasticity asymptotically approached unity as temperature increased.

Table 3
Average calibrated parameters values as denoted with an overbar.

Temperature (°C)	$\bar{\eta}$	$\bar{\alpha}$	$\bar{f}_0^{11}$	$\bar{f}_0^{12}$	$\bar{f}_0^{22}$	$\bar{\nu}$
23	624	0.637	0.717	−0.603	1.02	1.05
30	514	0.801	0.777	−0.576	0.871	0.982
40	491	0.897	0.698	−0.494	0.718	0.984
50	279	0.918	0.723	−0.456	0.609	0.866
60	277	0.942	0.471	−0.294	0.402	0.977

The next step of the model analysis entails propagating the uncertainty of the parameters through the model to quantify how well the output is described. A statistically significant number of samples are taken from the posterior densities and are used to generate 95% prediction and credible intervals. Fig. 3(a) shows the calibrated model response at 23°C. Additional calibration plots for the other tested temperatures can also be found in Fig. 3 where the same trends as with 23°C are seen.

An analysis measuring the error between the statistical model and the data is conducted using

$$e_{MCMC} = \frac{1}{N}\sum_{i=1}^{N}[s_3^{tot,data}(i) - s_3^{tot}(i;\theta)]^2 \tag{32}$$

where N is the number of data points, $s_3^{tot}(i;\theta)$ is the model stress response, and $s_3^{tot,data}(i)$ is the measured experimental stress which were all previously given in (29). The ℓ_2 norm error values at each temperature calibration are 1.99 kPa^2 for 23°C, 2.48 kPa^2 for 30°C, 0.954 kPa^2 for 40°C, 0.781 kPa^2 for 50°C, and 0.594 kPa^2 for 60°C.

We are also interested in assessing the effect of temperature on the excluded volume κ. To do this, we first look at fractional viscoelastic order (α) vs temperature in Fig. 4(a). The fractional viscoelastic order increases as temperature increases until it asymptotically approaches the limit of 1 (e.g., ideal linear dashpot). To relate the fractional order to the excluded volume, we use (28) and previously determined values of d_s=0.15 and d_f=1.87 (Mashayekhi et al., 2019). We can, therefore, transform Fig. 4(a) to show the excluded volume as a function of temperature which is plotted, along with its uncertainty due

Table 4
Standard deviations for calibrated parameters.

Temperature (°C)	σ_η	σ_α	$\sigma_{f_0^{11}}$	$\sigma_{f_0^{12}}$	$\sigma_{f_0^{22}}$	σ_ν
23	114	6.86×10^{-2}	5.08×10^{-2}	4.18×10^{-2}	9.69×10^{-2}	2.78×10^{-2}
30	58.1	8.92×10^{-2}	1.19×10^{-1}	5.99×10^{-2}	5.25×10^{-2}	5.06×10^{-2}
40	33.0	6.38×10^{-2}	7.65×10^{-2}	3.86×10^{-2}	3.00×10^{-2}	3.89×10^{-2}
50	19.3	6.16×10^{-2}	9.54×10^{-2}	5.30×10^{-2}	4.94×10^{-2}	4.63×10^{-2}
60	21.3	4.43×10^{-2}	4.02×10^{-2}	2.03×10^{-2}	1.80×10^{-2}	3.21×10^{-2}

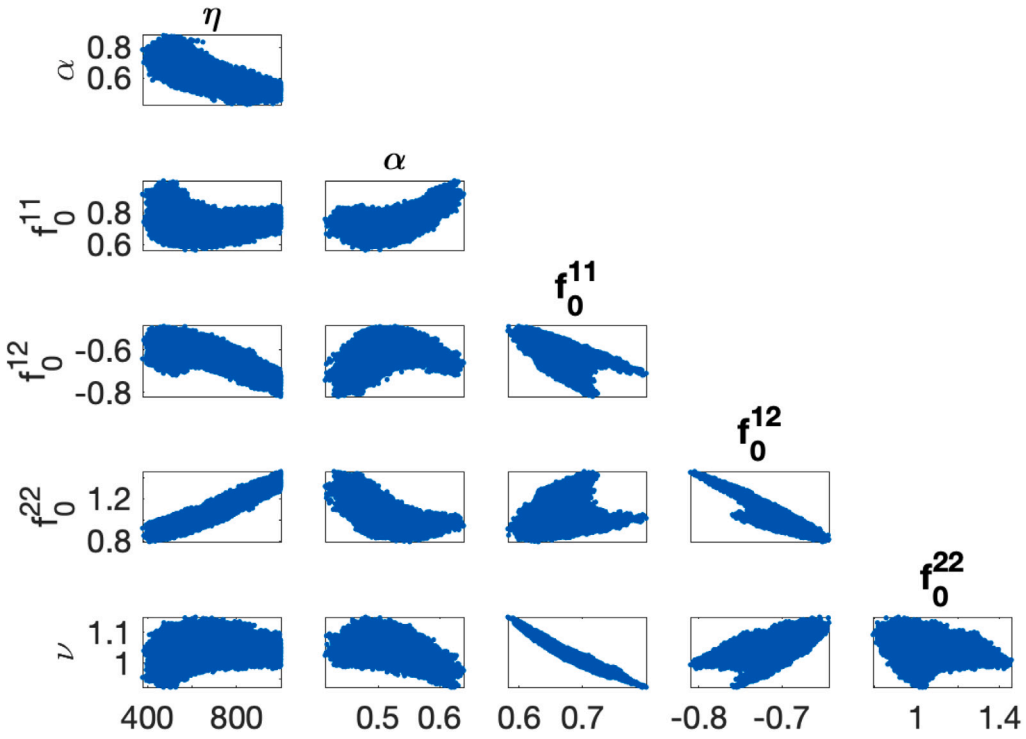

Fig. 2. Pairwise correlation plots for the parameters at T=23°C.

to uncertainty of α, in Fig. 4(b). As expected, the excluded volume follows the inverse trend as seen for fractional order vs temperature. The excluded volume decreases with increasing temperature until it hits an asymptote of approximately $\kappa \to -1.7$. Notably, its nominal value is negative which signifies net attraction between the monomers. This makes sense as VHB4905 is a solid so the monomers should be close together and entangled. A positive value for excluded volume would be more common in dilute solutions. Since elastomers tend to shrink when heated, this could explain the decrease in excluded volume.

Several fractal dimensions and fractal or fractional order operators have been used to better understand complex viscoelastic material behavior. While the direct relationship between these dimensions and operators remains elusive, we offer some discussion that may offer motivation for future work to simplify the modeling framework. We emphasize that the spectral dimension d_s and two dimensional fractal dimension d_f have been held constant over the temperature range tested. In prior work (Mashayekhi et al., 2019), we inferred the spectral dimension of VHB 4910, which has the same composition as VHB 4905, over comparable temperature ranges by measuring diffusion of temperature with an infrared camera. This would suggest a constant d_s is applicable here; however, prior infrared measurements were conducted at a zero strain state and thus neglected potential changes in the spectral dimension under different states of deformation. Similarly, the two dimensional fractal dimension was quantified at a zero strain state. Additional dependencies of strain on d_s and d_f should be investigated to understand the sensitivities of strain on the spectral and fractal dimensions. Moreover, we have made distinctions between the fractional order deformation constraint ν and any potential relations with the two dimensional fractal dimension d_f, the one dimensional fractal dimension ν in (2), and the fractal deformation gradient order β. Further work should be investigated to determine if direct relationships exist between the one, two, and three dimensional fractal geometry as a function of deformation and the gradient operators which estimate particle motion from some reference state.

4. Conclusions

A fractal inspired hyperelastic model is used to describe the reversible behavior of VHB4905 while a fractional order viscoelastic model is used to describe the viscoelastic behavior. The model is validated by comparing model fits to finite deformation experimental stress–stretch data over a range of temperatures. Surprisingly good model estimates are made by starting with an information theoretic approach that contains fractional order penalties on deformation. This constrains future deformation to follow a power-law function that is based on the fractal dimension of the polymer network in the undeformed Lagrangian frame. The additional assumption of time dependent covariance within this constraint illustrates how fractional order viscoelasticity emerges from the entropy generation function. By identifying a Bayesian posterior density and information entropy, we make use of prior research that connects information entropy to thermodynamic entropy and free energy expressions (Jaynes, 1957). Uncertainty methods are then used to obtain parameter value estimations given a sparse set of experimental data over a range of temperatures. The parameter values and their uncertainty for fractional order were related to the excluded volume in the interval from 23 °C to

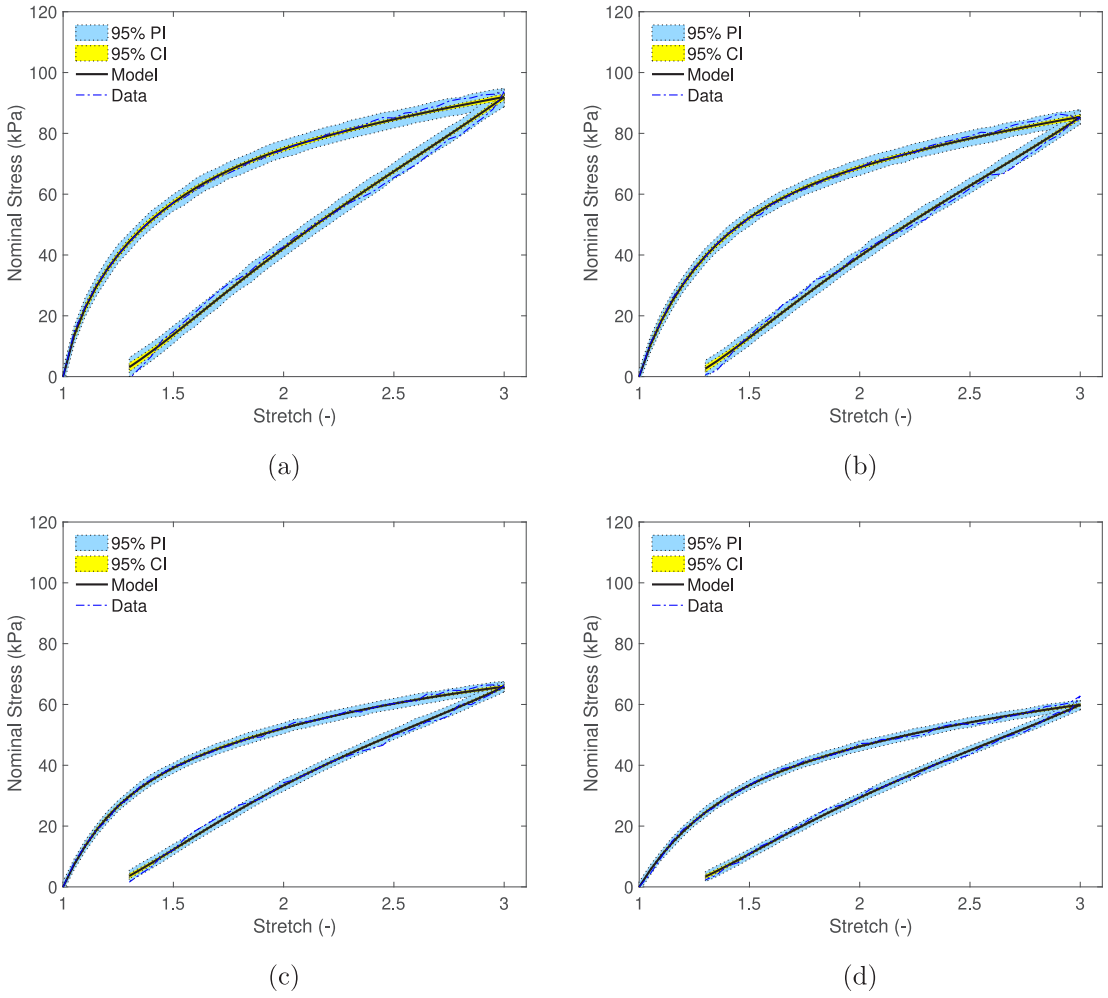

Fig. 3. Calibration plots. (a) T=23°C. (b) T=30°C. (c) T=50°C. (d) T=60°C. The plot calibrated at 40°C is not shown.

60 °C. A nominally decreasing to constant trend was inferred between the excluded volume and temperature given our model assumptions of fractal deformation and fractional order viscoelasticity. We note that the trend of α could be obscured by parameter correlations. Looking at the other parameters, f_0^{12} increases while f_0^{11} and f_0^{22} decrease. There could be underlying physical correlations between the fractional parameter ν and the excluded volume as well as temperature. Future work will focus on understanding differences between applying fractional time derivatives versus fractal order time derivatives to describe viscoelasticity to further validate the excluded volume trend as well as simplify model assumptions and computational complexity associated with non-local operators (fractional derivatives) vs. local operators (fractal derivatives) (Oldham and Spanier, 1974; Falconer, 2004).

CRediT authorship contribution statement

Eugenia Stanisauskis: Formal analysis, Investigation, Methodology, Validation, Visualization, Writing – original draft, Writing – review & editing. **Somayeh Mashayekhi:** Formal analysis, Investigation, Methodology, Writing – review & editing. **Basanta Pahari:** Conceptualization, Formal analysis, Investigation, Methodology, Writing – review & editing. **Markus Mehnert:** Data curation, Writing – review & editing. **Paul Steinmann:** Formal analysis, Writing – review & editing. **William Oates:** Conceptualization, Formal analysis, Funding acquisition, Investigation, Methodology, Project administration, Resources, Supervision, Writing – original draft, Writing – review & editing.

Declaration of competing interest

The authors declare that they have no known competing financial interests or personal relationships that could have appeared to influence the work reported in this paper.

Acknowledgments

The research of WSO was supported in part by the Department of Defense Basic Research Program for HBCU/MI (W911NF-19-S-0009). ELS acknowledges support from the Department of Defense SMART Scholarship. SM was partially supported by the National Science Foundation grant DBI 2109990.

Appendix

We provide details on the choice of differential operators for our deformation gradient introduced in Section 2. Following Tarasov (2011), we define the fractal measure on a collection of 3 measurable sets (W_k, μ_k, D) with $k = 1, 2, 3$ to form the Cartesian product set $W = W_1 \times W_2 \times W_3$. Here, μ_k is the measure in each Cartesian direction and $D \leq 3$ is the fractal volume dimension. The fractal measure over this set is

$$\mu_B(W) = \mu_1(W_1)\mu_2(W_2)\mu_3(W_3) \tag{33}$$

and we can evaluate a function over the fractal domain

$$\int_W f(\overline{x}_1, \overline{x}_2, \overline{x}_3) d\mu_B = \int_{W_1}\int_{W_2}\int_{W_3} f(\overline{x}_1, \overline{x}_2, \overline{x}_3) d\mu_1(\overline{x}_1) d\mu_2(\overline{x}_2) d\mu_3(\overline{x}_3)$$

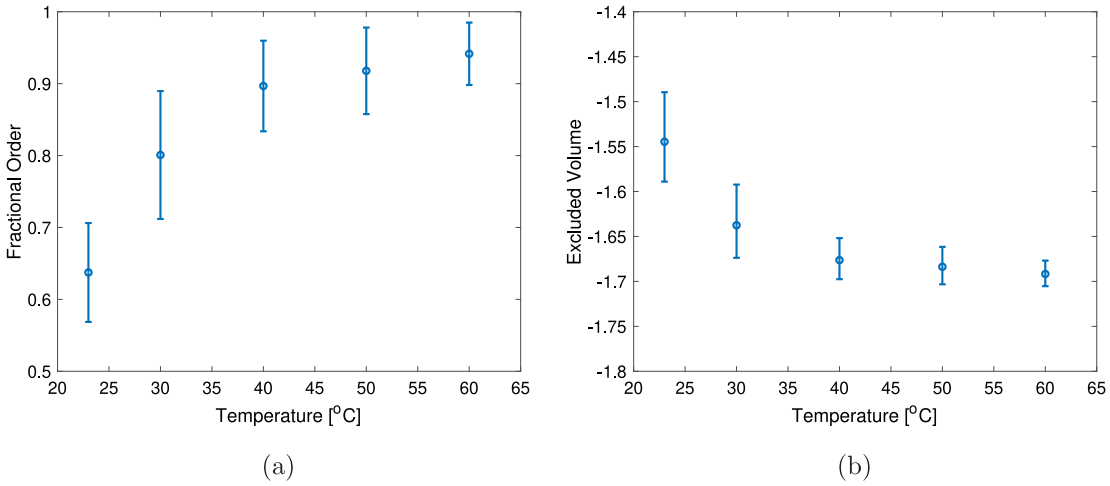

Fig. 4. (a) Fractional order vs. temperature including the 95% credible intervals of the fractional order α. (b) The corresponding excluded volume (κ) according to (28).

(34)

where we have introduced a normalized set of coordinates in the Eulerian frame, $\overline{x}_k = x_k/l_0$ where l_0 is the characteristic length scale. We will use this length scale later when homogenizing the fractal structure as an effective continuum.

We divide the fractal volume measure into an estimate of fractal dimensions along each Cartesian direction which quantifies the fractal dimension for each W_k. In this analysis, we assume isotropy in the fractal dimensions which further allows

$$D = \nu_1 + \nu_2 + \nu_3 = 3\nu \tag{35}$$

where $\nu = \nu_1 = \nu_2 = \nu_3$.

The relationship between the fractal measure in each direction (μ_i) and the Cartesian (Eulerian) direction $\overline{x}_i$ is defined to be

$$\mu_i(\overline{x}_i) = \frac{\pi^{\nu/2}}{2^\nu \Gamma(\nu/2+1)} |\overline{x}_i|^\nu \tag{36}$$

where $\Gamma(\nu/2+1)$ is the Gamma function. This functional relationship describes a length measure of the fractal specifically along the direction $\overline{x}_i$ where the subscript i on μ_i corresponds to the $\overline{x}_i$ direction.

Given the power law relation in (36), we evaluate kinematic relations where we approximate deformation gradients over the fractal measure $\mu_i(\overline{x}_i)$ to quantify relative changes in particle distances. These measures of relative displacement must be invariant to rigid body translations and rotations which poses challenges over the fractal metric given by (36). This challenge is due to the lack of translational and rotational invariance at a point (Tarasov, 2011). Micropolar theory has been proposed to address the rotational invariance problem for the case of anisotropic fractals (Li and Ostoja-Starzewski, 2020). However, issues remain, even in the isotropic fractal case, that we discuss as follows.

We take the approach of defining a homogenized measure of deformation over a finite set instead of taking the limit to a continuum point. This creates a trade-off in spatial accuracy at a continuum point with a more accurate measure that is invariant to translations and rotations. Despite this trade-off, it is expected to provide a better measure for predicting kinematics that accommodate material complexities that do not follow Gaussian distributions. In the following derivation, we outline the approach and assumptions used to approximate deformation gradients over a finite set which homogenizes the underlying fractal structure. We also note that it is not the only operator that may be considered. Many others may also be considered which may provide enhanced estimates for specific material characteristics (Atangana, 2017).

We first take the differential of (36)

$$\frac{d\mu_i}{d\overline{x}_i^\beta} = \frac{d}{d\overline{x}_i^\beta}\left(|\overline{x}_i|^\nu\right)\frac{\pi^{\nu/2}}{2^\nu\Gamma(\nu/2+1)} = \frac{1}{\beta\overline{x}_i^{\beta-1}}\frac{d}{dx_i}\left(|\overline{x}_i|^\nu\right)\frac{\pi^{\nu/2}}{2^\nu\Gamma(\nu/2+1)}$$
$$= \frac{\mathrm{sgn}(\overline{x}_i)\pi^{\nu/2}}{2^\nu\Gamma(\nu/2+1)}\frac{\nu|\overline{x}_i|^{\nu-1}}{\beta\overline{x}_i^{\beta-1}} \tag{37}$$

where we applied the fractal derivative in the second step. Also note that we only take the derivative in directions aligned between the measure μ_i and $\overline{x}_i$ since the fractal measure in (36) is only defined in these directions.

If $\nu = \beta$ and $\overline{x}_i > 0$, we have

$$d\mu_i = \frac{\pi^{\nu/2}}{2^\nu\Gamma(\nu/2+1)} d\overline{x}_i^\nu. \tag{38}$$

We now evaluate the fractal Eulerian differential $d\overline{x}_i^\nu$ by evaluating its change with respect to the Lagrangian frame. We do this by first noting that $\overline{x}_i = \overline{x}_i(\overline{X}_K)$ where we define a similar normalization in the Lagrangian frame, $\overline{X}_K = X_K/L_0$, given the characteristic length L_0 in the Lagrangian frame. This power law differential along the i direction is $d\overline{x}_i^\nu = \nu\overline{x}_i^{\nu-1}d\overline{x}_i = \nu\overline{x}_i^{\nu-1}\frac{\partial\overline{x}_i}{\partial\overline{X}_K}d\overline{X}_K$ where there is no sum on i. In the last step, the chain rule was applied on $\overline{x}_i = \overline{x}_i(\overline{X}_K)$.

We can now return to (37) and expand the more general relation where $\nu \neq \beta$. For $\overline{x}_i > 0$, the fractal differential is

$$d\mu_i = \frac{\pi^{\nu/2}\nu}{2^\nu\Gamma(\nu/2+1)}\frac{|\overline{x}_i|^{\nu-1}}{\beta\overline{x}_i^{\beta-1}}d\overline{x}_i^\beta = \frac{\pi^{\nu/2}\nu}{2^\nu\Gamma(\nu/2+1)}\frac{|\overline{x}_i|^{\nu-1}}{\beta\overline{x}_i^{\beta-1}}\beta\overline{x}_i^{\beta-1}\overline{F}_{iK}d\overline{X}_K \tag{39}$$

where $\overline{F}_{iK}d\overline{X}_K = \frac{\partial\overline{x}_i}{\partial\overline{X}_K}d\overline{X}_K$. If we let

$\overline{F}_{iK}d\overline{X}_K = \frac{\partial\overline{x}_i}{\partial\overline{X}_K}d\overline{X}_K = \frac{1}{l_0}\frac{\partial x_i}{\partial X_K}dX_K := \frac{1}{l_0}F_{iK}dX_K$ and $\nu = \beta$, this simplifies to

$$d\mu_i = \frac{\pi^{\nu/2}\nu|x_i|^{\nu-1}}{2^\nu l_0^{\nu-2}\Gamma(\nu/2+1)}F_{iK}dX_K. \tag{40}$$

Since we have assumed isotropy in the fractal metric, spherical symmetry can be applied. Translational and rotational invariance is established by restricting the radius of some sphere to a finite set that we define by the characteristic length $|x_i| = l_0$ where the originally defined l_0 defines a representative continuum volume element of sufficient size to represent the fractal structure. In principle, this characteristic scale could be determined using the box-count method and evaluating the uncertainty of the fractal dimension as the box size shrinks to l_0. By defining $|x_i| = l_0$, this means we have set the operating point about the

fractal derivative and the chain rule to be about l_0. This gives the final relation

$$d\mu_i = \frac{\pi^{\nu/2}}{2^{\nu-1} l_0 \Gamma(\nu/2)} F_{iK}\, dX_K \tag{41}$$

such that the fractal deformation gradient scales with the Euclidean deformation gradient according to

$$F^{\nu}_{iK} = \frac{\pi^{\nu/2}}{2^{\nu-1} l_0 \Gamma(\nu/2)} F_{iK}. \tag{42}$$

It is important to note the normalization of length on the fractal deformation gradient relative to the Euclidean deformation gradient. This is because we have normalized the fractal displacement metric in (36). In the limit of $\nu \to 1$, the fractal deformation gradient equals the Euclidean deformation gradient if $l_0 = 1$ (unitless given the unitless fractal measure in (36)). If $0 < \nu < 1$, the fractal deformation gradient is scaled by the appropriate characteristic length scale of the representative volume element and the Gamma function.

References

Alexander, S., Orbach, R., 1982. Density of states on fractals:fractons. J. Phys. Lett. 43 (17), 625–631.

Atangana, A., 2017. Fractal-fractional differentiation and integration: connecting fractal calculus and fractional calculus to predict complex system. Chaos Solitons Fractals 102, 396–406.

Balankin, A.S., 2015. A continuum framework for mechanics of fractal materials I: from fractional space to continuum with fractal metric. Eur. Phys. J. B 88 (4), 90.

Balankin, A.S., Mena, B., Martinez-Gonzalez, C.L., Matamoros, D.M., 2012. Random walk in chemical space of cantor dust as a paradigm of superdiffusion. Phys. Rev. E 86 (5), http://dx.doi.org/10.1103/physreve.86.052101.

Caticha, A., 2015. Entropic dynamics. Entropy 17 (9), 6110–6128.

Caticha, A., Preuss, R., 2004. Maximum entropy and Bayesian data analysis: Entropic prior distributions. Phys. Rev. E 70 (4), 046127.

Chen, W., Sun, H., Zhang, X., Korošak, D., 2010. Anomalous diffusion modeling by fractal and fractional derivatives. Comput. Math. Appl. 59 (5), 1754–1758.

Chen, W., Wang, F., Zheng, B., Cai, W., 2017. Non-euclidean distance fundamental solution of hausdorff derivative partial differential equations. Eng. Anal. Bound. Elem. 84, 213–219.

Falconer, K., 2004. Fractal Geometry: Mathematical Foundations and Applications. John Wiley & Sons.

Haario, H., Laine, M., Mira, A., Saksman, E., 2006. DRAM: Efficient adaptive MCMC. Stat. Comput. 16 (4), 339–354. http://dx.doi.org/10.1007/s11222-006-9438-0.

Haario, H., Saksman, E., Tamminen, J., 2001. An adaptive Metropolis algorithm. Bernoulli 7 (2), 223–242.

Havlin, S., Ben-Avraham, D., 1987. Diffusion in disordered media. Adv. Phys. 36 (6), 695–798.

Jaynes, E.T., 1957. Information theory and statistical mechanics. Phys. Rev. 106 (4), 620.

Jaynes, E., 1965. Gibbs vs Boltzmann entropies. Amer. J. Phys. 33 (5), 391–398. http://dx.doi.org/10.1119/1.1971557.

Li, J., Ostoja-Starzewski, M., 2009. Fractal solids, product measures and fractional wave equations. Proc. R. Soc. A Math. Phys. Eng. Sci. 465 (2108), 2521–2536.

Li, J., Ostoja-Starzewski, M., 2013. Comment on "hydrodynamics of fractal continuum flow" and "map of fluid flow in fractal porous medium into fractal continuum flow". Phys. Rev. E 88 (5), 057001.

Li, J., Ostoja-Starzewski, M., 2020. Thermo-poromechanics of fractal media. Phil. Trans. R. Soc. A 378 (2172), 20190288.

Lischke, A., Pang, G., Gulian, M., Song, F., Glusa, C., Zheng, X., Mao, Z., Cai, W., Meerschaert, M.M., Ainsworth, M., et al., 2020. What is the fractional Laplacian? A comparative review with new results. J. Comput. Phys. 404, 109009.

Malvern, L., 1969. Introduction to the Mechanics of a Continuous Medium. Prentice-Hall, Inc. Englewood Cliffs, NJ.

Mandelbrot, B.B., Evertsz, C.J., Gutzwiller, M.C., 2004. Fractals and Chaos: the Mandelbrot Set and Beyond, Vol. 3. Springer.

Mashayekhi, S., Hussaini, M.Y., Oates, W., 2019. A physical interpretation of fractional viscoelasticity based on the fractal structure of media: Theory and experimental validation. J. Mech. Phys. Solids 128, 137–150.

Mashayekhi, S., Miles, P., Hussaini, M.Y., Oates, W.S., 2018. Fractional viscoelasticity in fractal and non-fractal media: Theory, experimental validation, and uncertainty analysis. J. Mech. Phys. Solids 111, 134–156.

Mashayekhi, S., Stanisauskis, E., Hassani, M., Oates, W., 2021. Excluded volume effects and fractional viscoelasticity in polymers. Meccanica 1–12.

Mehnert, M., Hossain, M., Steinmann, P., 2021. A complete thermo-electro-viscoelastic characterization of dielectric elastomers, Part I: Experimental investigations. J. Mech. Phys. Solids 157, 104603. http://dx.doi.org/10.1016/j.jmps.2021.104603.

Miles, P., Hays, M., Smith, R., Oates, W., 2015. BayesIan uncertainty analysis of finite deformation viscoelasticity. Mech. Mater. 91, 35–49.

Miloevic, N.T., Elston, G.N., Krstonoic, B., Rajkovic, N., 2013. Box-count analysis of two dimensional images: Methodology, analysis and classification. In: 2013 19th International Conference on Control Systems and Computer Science. IEEE, pp. 306–312. http://dx.doi.org/10.1109/cscs.2013.16.

Oates, W., Stanisaukis, E., Pahari, B.R., Mashayekhi, S., 2021. Entropy dynamics approach to fractional order mechanics with applications to elastomers. In: Behavior and Mechanics of Multifunctional Materials XV, Vol. 11589. International Society for Optics and Photonics, 1158905.

Oates, W.S., Stanisauskis, E., Solheim, H., Miles, P., 2018. Fractional viscoelasticity of soft elastomers and auxetic foams. In: Behavior and Mechanics of Multifunctional Materials and Composites XII. http://dx.doi.org/10.1117/12.2296666.

Oldham, K., Spanier, J., 1974. The Fractional Calculus Theory and Applications of Differentiation and Integration to Arbitrary Order. Elsevier.

Pahari, B.R., Oates, W., 2022. Renyi entropy and fractional order mechanics for predicting complex mechanics of materials. In: Behavior and Mechanics of Multifunctional Materials XVI, Vol. 12044. SPIE, International Society for Optics and Photonics, pp. 49–57.

Rubinstein, M., Colby, R.H., et al., 2003. Polymer Physics, Vol. 23. Oxford University Press, New York.

Smith, R., 2013. Uncertainty Quantification : Theory, Implementation, and Applications. Society for Industrial and Applied Mathematics, Philadelphia.

Sumelka, W., 2014. Thermoelasticity in the framework of the fractional continuum mechanics. J. Therm. Stresses 37 (6), 678–706.

Tadmor, E.B., Miller, R.E., 2011. Modeling Materials: Continuum, Atomistic and Multiscale Techniques. Cambridge University Press.

Tarasov, V.E., 2005. Continuous medium model for fractal media. Phys. Lett. A 336 (2–3), 167–174.

Tarasov, V.E., 2011. Fractional Dynamics: Applications of Fractional Calculus to Dynamics of Particles, Fields and Media. Springer Science & Business Media.

Weiner, J.H., 2012. Statistical Mechanics of Elasticity. Courier Corporation.

West, B., Bologna, M., Grigolini, P., 2012. Physics of Fractal Operators. Springer Science & Business Media.

West, B.J., Grigolini, P., 2010. Complex Webs: Anticipating the Improbable. Cambridge University Press.

Wheatcraft, S.W., Meerschaert, M.M., 2008. Fractional conservation of mass. Adv. Water Resour. 31 (10), 1377–1381.